FEBS Letters 589 (2015) 84–88

journal homepage: www.FEBSLetters.org

# A potential function for neuronal exosomes: Sequestering intracerebral amyloid-β peptide

Kohei Yuyama [a,*], Hui Sun [a], Seigo Usuki [a], Shota Sakai [a], Hisatoshi Hanamatsu [a], Tetsuo Mioka [a,b], Nobuyuki Kimura [c], Megumi Okada [d], Hidetoshi Tahara [d], Jun-ichi Furukawa [e], Naoki Fujitani [e], Yasuro Shinohara [e], Yasuyuki Igarashi [a]

[a] Laboratory of Biomembrane and Biofunctional Chemistry, Graduate School of Advanced Life Science, and Frontier Research Center for Post-Genome Science and Technology, Hokkaido University, Sapporo, Japan
[b] Division of Molecular Interaction, Institute for Genetic Medicine, Graduate School of Life Science, Hokkaido University, Sapporo, Japan
[c] Section of Cell Biology and Pathology, Department of Alzheimer's Disease Research, Center for Development of Advanced Medicine for Dementia, National Center for Geriatrics and Gerontology, Obu, Japan
[d] Department of Cellular and Molecular Biology, Graduate School of Biomedical Science, Hiroshima University, Hiroshima, Japan
[e] Laboratory of Medical and Functional Glycomics, Graduate School of Advanced Life Science, and Frontier Research Center for Post-Genome Science and Technology, Hokkaido University, Sapporo, Japan

ARTICLE INFO

*Article history:*
Received 24 September 2014
Revised 7 November 2014
Accepted 19 November 2014
Available online 29 November 2014

Edited by Jesus Avila

*Keywords:*
Exosome
Amyloid-β peptide
Alzheimer's disease
Cynomolgus monkey
APP transgenic mouse
Cerebrospinal fluid

ABSTRACT

**Elevated amyloid-β peptide (Aβ) in brain contributes to Alzheimer's disease (AD) pathogenesis. We demonstrated the presence of exosome-associated Aβ in the cerebrospinal fluid (CSF) of cynomolgus monkeys and APP transgenic mice. The levels of exosome-associated Aβ notably decreased in the CSF of aging animals. We also determined that neuronal exosomes, but not glial exosomes, had abundant glycosphingolipids and could capture Aβ. Infusion of neuronal exosomes into brains of APP transgenic mice decreased Aβ and amyloid depositions, similarly to what reported previously on neuroblastoma-derived exosomes. These findings highlight the role of neuronal exosomes in Aβ clearance, and suggest that their downregulation might relate to Aβ accumulation and, ultimately, the development of AD pathology.**


## 1. Introduction

A pathological feature of Alzheimer's disease (AD) is the presence of senile plaques, extracellular amyloid depositions of amyloid-β peptide (Aβ). Aβ is generated by the processing of amyloid precursor protein (APP), and is maintained at a steady state in normal brain. However, disruption of the balance in Aβ metabolism contributes to the formation of toxic Aβ assemblies and amyloid depositions, which are linked to AD pathogenesis. Recently, exosomes, a subtype of secreted vesicles, were reported to associate with extracellular Aβ in cultures of APP-expressing neuroblastoma cells [1,2]. Similarly, our previous study both in vitro and in vivo demonstrated that exosomes released from neuroblastoma N2a can bind Aβ on their surface glycosphingolipids (GSLs) and these Aβ-bound exosomes are then internalized by microglia for degradation [3,4]. This suggests that N2a-derived exosomes may act for Aβ elimination in brain. However, it remains unclear whether the exosomes, which originate from cells resident in the central nervous system, also contribute to Aβ metabolism.

## 2. Materials and methods

### 2.1. Animals

Wild type C57BL/6 mice and mice expressing the human APP bearing the Swedish and Indiana (KM670/671NL, V717F) mutations (J20) were obtained from SLC Inc. (Hamamatsu, Japan) and the Jackson Laboratory (Bar Harbor, ME), respectively. All

*Abbreviations:* Aβ, amyloid-β peptide; AD, Alzheimer disease; APP, amyloid-β precursor protein; GSL, glycosphingolipid; CSF, cerebrospinal fluid; N2a, neuro2a; EGCase, endoglycoceramidase

* Corresponding author.
*E-mail address:* kyuyama@pharm.hokudai.ac.jp (K. Yuyama).

http://dx.doi.org/10.1016/j.febslet.2014.11.027
0014-5793/

animal procedures were approved by the Animal Care Committees of Hokkaido University.

### 2.2. Monkey and murine samples

Cynomolgus monkeys (*Macaca fascicularis*) were housed at the Tsukuba Primate Research Center (TPRC), National Institute of Biomedical Innovation (NIBIO), Ibaraki, Japan. Monkey CSF samples were obtained by lumbar puncture. Nine CSF samples were from young monkeys (4–8 years old), 8 from adult monkeys (11–21 years old), and 4 from aged monkeys (24–36 years old). Each CSF sample was used for exosome isolation without prior freezing. The parietal lobes of 20 monkeys were used for Western blotting and ELISA. All animals were bred and maintained in an air-conditioned room at the TPRC with controlled illumination (12 h light/12 h dark), temperature (25 ± 2 °C), humidity (60 ± 5%), and ventilation (10 cycles/h), and were given 70 g of commercial food and 100 g of apples daily, with unlimited access to tap water [5]. The maintenance of animals was conducted according to rules of the TPRC at NIBIO regarding the care, use, and biohazard countermeasures of laboratory animals. All animal experiments were conducted according to the guidelines of the Animal Care and Use Committee of the NIBIO, Japan.

Mouse CSF was sampled from the cisterna magna following protocols previously reported [6]. Each 50 μl of CSF was collected from 2-month-old C57BL/6 mice or APP mice at the indicated ages.

### 2.3. Cell cultures

Primary neuron cultures were prepared from the cerebral cortices of mouse brains on embryonic day 15 as described previously [3]. Primary glial cultures were prepared from the mouse cortices according to published methods with minor modifications [7,8]. Briefly, the neocortex was removed from each 2-day-old mouse pup, dissociated in a dissociation solution (Sumitomo Bakelite, Tokyo, Japan), and plated in DMEM and 10% fetal bovine serum (FBS). After being cultured for 14 days, the microglia were detached by shaking, and the separate cells were cultured in DMEM/5% FBS. The astrocytes remaining in the flasks were cultured in DMEM/10% FBS. The resultant glial cells were cultured for two days and used for further analysis.

### 2.4. Exosome isolation

Exosomes were prepared from supernatants of primary cultures as described previously [3]. Briefly, after culture of cells for one day, the culture supernatants were sequentially centrifuged at 2000×*g* for 10 min, and at 10000×*g* for 30 min, and at 100000×*g* for 1 h to obtain exosomes as pellets. Using this same method, exosomes were also isolated from the CSF samples of APP mice or monkeys.

### 2.5. Electron microscopy

Exosomes were stained with phosphotungstic acid. For immunolabeling, the exosomes were incubated with anti-Aβ antibody (4G8) then 10 nm gold-coupled anti-IgG. Images were taken with JEM-ARM200F (JEOL Ltd., Tokyo, Japan) transmission electron microscope.

### 2.6. Western blotting

To detect target proteins, we employed monoclonal antibodies against Alix, GM130, Transferrin receptor (BD Biosciences), and Aβ (6E10, Signet, Dedham, MA), and a polyclonal antibody against flottilin-1 (Santa Cruz Biotechnology). Ganglioside GM1, was detected by cholera toxin B subunit (Sigma).

### 2.7. Fluorescence labeling for the exosomes

Labeling of the exosomes was performed using PKH26 (Sigma) as described previously [3].

### 2.8. Analysis of particle size and number

The exosomes collected from primary cultures of neurons and CSF samples were suspended in PBS, and a qNano System (Izon Science, Ltd) employed to analyze the particle size and densities. CPC100 was used as the calibration sample.

### 2.9. Exosome administration into mouse brains

The experiment was performed as previously described [4]. Briefly, mice were continuously treated with exosomes (2 mg protein/ml) or PBS by Alzet minipump at 0.25 μl/h for 14 days. The Brain Infusion Kit was implanted into the right hippocampus using a stereotactic instrument. One hemibrain was fixed for immunohistochemistry, and the other was frozen for use in ELISA.

### 2.10. Immunohistochemistry and thioflavin-S (ThS) staining

Immunostaining and ThS staining were performed as described previously [4].

### 2.11. Aβ ELISA

$A\beta_{1-40}$ and $A\beta_{1-42}$ levels were determined using an ELISA kit (Wako, Osaka, Japan) as previously described [4].

### 2.12. Measurement of glycosphingolipids (GSLs)

Levels of GSLs in the exosomes of primary cultures were measured as described previously [4]. After their extraction, the GSLs were enzymatically digested with EGCase I and II, further purified by glycoblotting, then analyzed by MALDI-TOF MS.

### 2.13. Endoglycosylceramidase (EGCase)

Exosomes (1 mg protein/ml) were incubated with 0.5 U/ml EGCase II (Takara Bio Inc., Shiga, Japan) at 37 °C for 15 h in PBS.

### 2.14. Thioflavin assay

Thioflavin-T (ThT) assay was performed as previously published [4].

### 2.15. Aβ binding assay

Fluorescent $A\beta_{1-42}$ (25 μM) was incubated with the PKH26-labeled exosomes (treated with or without EGCase) in serum-free medium at 37 °C for 5 h. The exosomes and bound Aβ were observed after wash out free Aβ.

## 3. Results

### 3.1. Exosomes associate with Aβ in the CSF of non-human primates

The non-human primate cynomolgus monkey is widely used for AD-related preclinical studies [9]. In the monkey brains, Aβ naturally increases in an age-dependent manner (Fig. 1A) as described in the

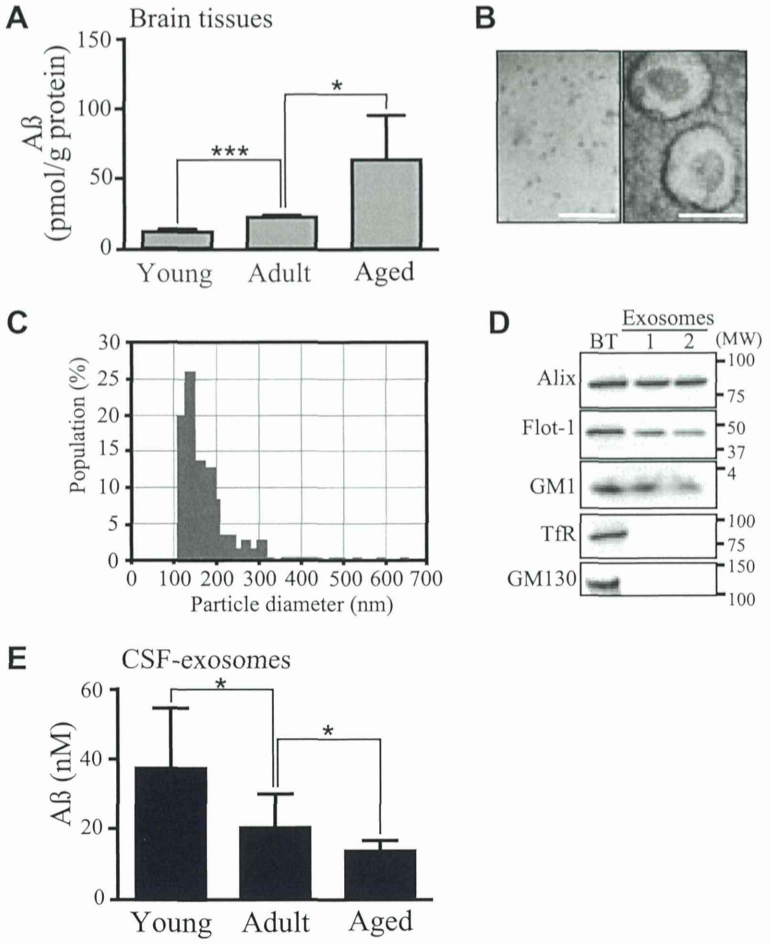


**Fig. 1.** Exosomes associate with Aβ in the CSF of cynomolgus monkeys. (A) Aβ levels in the brain tissues were analyzed. Values are presented as the mean ± S.D. (Young, $n = 5$; Adult, $n = 6$; Aged, $n = 9$, $^{*}P < 0.05$, $^{***}P < 0.001$). (B) Images of the exosome fraction. Bars: 1 μm in left panel, 100 nm in right panel. (C) Particle size distribution of the exosome fraction. (D) Western blotting of the exosomes. Alix, flotillin-1(Flot-1), and ganglioside GM1 (GM1) as exosome markers; transferrin receptor (TfR) and GM130 as negative markers. BT, brain tissues (E) Aβ levels in the CSF-exosomes were measured. Values are presented as the mean ± S.D. (Young, $n = 9$; Adult, $n = 8$; Aged, $n = 4$, $^{*}P < 0.05$).

previous reports [10,11]. To investigate the effect of exosomes originating from brain cells against Aβ metabolism, we isolated exosomes from monkey CSF, then measured the Aβ levels in the exosome fractions. The CSF-derived exosomes were confirmed by electron microscopy to mainly consist of small membrane vesicles 50–200 nm in diameter (Fig. 1B), similar to previously described [12]. The exosome size was further verified by a nanoparticle analyzer, which found the sizes to range from 100 to 200 nm (Fig. 1C). The exosomal markers were also identified in the CSF-exosome fractions (Fig. 1D). We found that Aβ was detectable in all CSF-derived exosome fractions but that the levels of exosome-associated Aβ were markedly lower in the adult and aged brains compared to the young subjects (Fig. 1E). The level of free Aβ, which was not associated with the exosomes in the CSF, declined only in the aged brains (Supplemental Fig. 1). These results suggest that the function of exosomes transporting Aβ in the central nervous system may deteriorate with age (>11-year-old).

### *3.2. Age-related alterations in the number of exosomes in primary neuronal cultures and APP transgenic mouse CSF*

Neuronal cell cultures are widely used as models to study the molecular mechanisms of aging. We collected the exosomes from primary cultures of cortical neurons at 1, 7, or 14 day in vitro (DIV) and found that there were significant reductions in the number of particles at DIV14 compared to those at DIV1 or DIV7 (Supplemental Fig. 2A). While exosomal GSLs, especially sialylated GSLs, kept rising up to DIV14 (Supplemental Fig. 2B). These suggest that a reduction in exosome release might occur during aging, with maintaining the capacity of individual exosome to bind with Aβ.

To investigate whether the above findings in the non-human primates and in the neuronal cultures are also observed in APP transgenic mice, we collected the exosomes from CSF of 13-month-old APP mice and examined them for the presence of Aβ, using western blot analysis and electron microscopy with immunolabeling (Fig. 2A and B). We then quantified the exosomes isolated from APP mouse CSF at ages 2 to 23 months. Compared to the number of CSF-exosomes isolated from young mice (2–3 months old), the densities of exosomes in mice aged 6–7 months decreased; these low levels were maintained through 12–13 months of age, thereafter drastically declined in 23-month-old mice (Fig. 2C). We also showed marked reduction in Aβ levels in the CSF-exosomes between 2- and 23-month-old APP transgenic mice (2.19 ± 0.36 nM and 0.015 ± 0.012 nM, respectively), in accordance with those in the monkey CSF with age. In contrast, Aβ levels in the brain tissues continued rising in mice from ages 6–7 months to 23 months. The above data raised the possibility that endogenous exosomes released from brain cells may play a role in modulating Aβ metabolism.

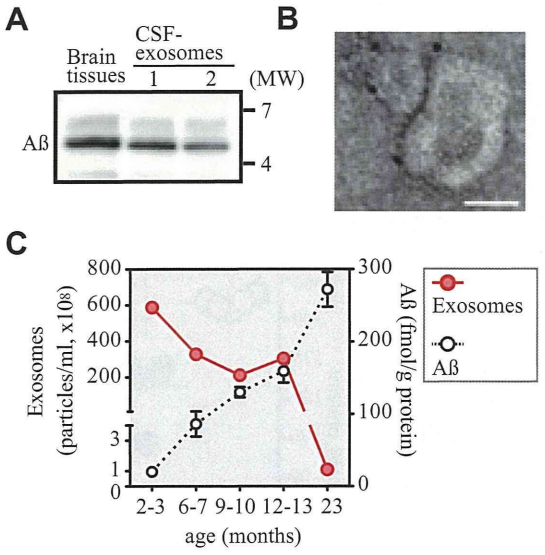


**Fig. 2.** Age-dependent alterations in the concentrations of exosomes from APP mouse CSF. (A) Aβ in whole brain tissues (5 μg protein) and in exosomes isolated from the CSF (50 μl) of 13-month-old APP mice was detected. (B) Exosomes derived from 13-month-old APP mouse CSF were negatively stained and immunolabeled for Aβ. Scale bar, 50 nm. (C) CSF was collected from APP mice at the indicated ages, and the densities of the exosomes were measured. Aβ levels in whole brains of APP mice were quantified. Values of Aβ levels are presented as the mean ± S.D. ($n = 5$).

### 3.3. GSL-enriched neuronal exosomes, but not glial exosomes, associate with Aβ

We previously determined that the enriched glycans of the GSLs are essential for Aβ binding and assembly on N2a-exosomes [3]. To examine this in our current model, we collected exosomes from primary cultures of rodent cortical neurons, astrocytes and microglia, and determined the profiles of their GSL-derived glycans and their propensity for trapping Aβ. We found that there were significantly more GSLs in neuronal exosomes than in exosomes from glial cells (Fig. 3A). Sialylated GSLs were also abundant in the neuronal exosomes; in particular, trisialoganglioside GT1 was found in only neuronal exosomes (Supplemental Table 1). Ganglioside GM1, which has been reported to bind Aβ in AD brains, was also highly enriched in neuronal exosomes (Supplemental Fig. 3 and Table 1). Accordingly, neuronal exosomes, but not glial exosomes, associated with Aβ (Fig. 3B). In ThT assays for amyloid fibril detection, fluorescence intensities were enhanced after a 5 h-incubation with Aβ (Fig. 3C). Pretreatment of the neuronal exosomes with EGCase largely prevented the ThT fluorescence (Fig. 3C), indicating that the GSLs abundant in the neuronal exosomes contributed to the potency of the exosomes to bind Aβ.

### 3.4. Administration of neuronal exosomes decreases Aβ pathology in APP mouse brains

To assess the effect of the exosomes derived from primary neurons on amyloid pathology, we continuously administered the exosomes into the right hippocampus of 13-month-old APP mice. We found that the exosomes induced marked reductions in Aβ immunoreactive burdens (Fig. 4A and B) and ThS-positive plaques (Fig. 4C) in the treated hippocampus. Tissue levels of Aβs were also significantly decreased following the exosome infusion (Fig. 4D). These findings demonstrate that the treatment with neuronal exosomes effectively ameliorates Aβ pathology in APP mice, suggesting a novel role for neuronal exosomes in clearing Aβ in brain.

## 4. Discussion

Our study shown here demonstrated that exosomes are presented in monkey and murine CSF. The exosomes collected from monkey CSF at all ages contained Aβ (Fig. 1E), demonstrating that endogenous exosomes are also coupled with Aβ. In addition, the numbers of exosomes in the CSF of APP transgenic mice changed in an age dependent manner (Fig. 2C). It remains unclear which age-related factors would modulate exosome numbers, although the impairment of endocytic transport might be a potent possibility. Endocytic disturbances, such as endosome enlargement, are observed in aged monkey brains, with concomitant higher

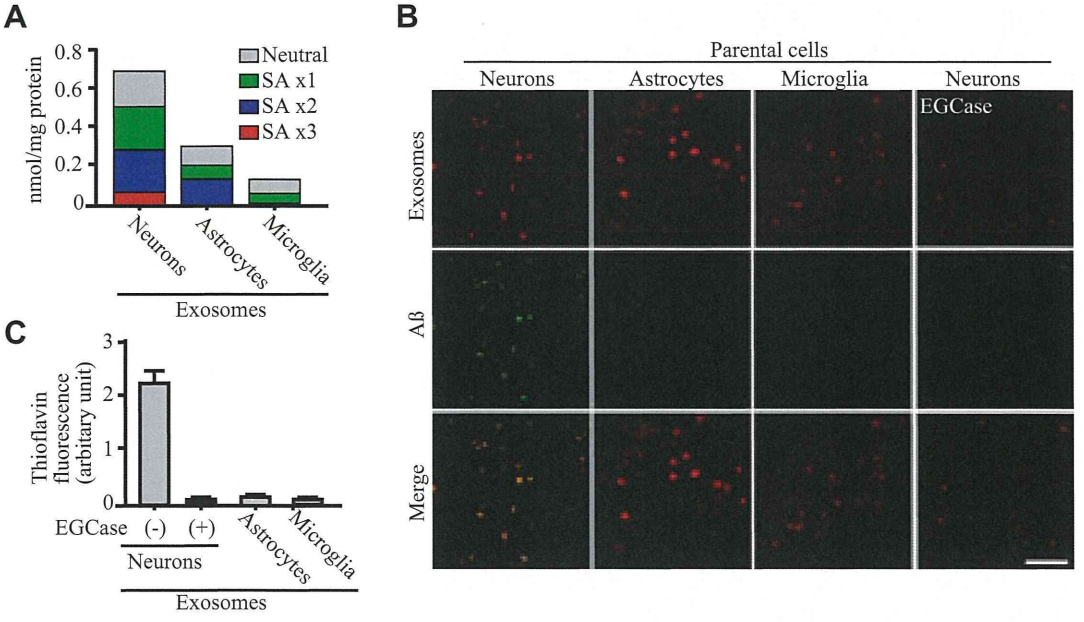


**Fig. 3.** GSL-enriched neuronal exosomes associate with Aβ. Exosomes were collected from primary cultures of cortical neurons (DIV7), astrocytes, and microglia. (A) Total amounts of GSL-glycans and the number of sialic acid moieties in the exosomes were measured. (B) Representative images of fluorescent Aβ binding on exosomes after a 5 h exposure. Bar, 100 μm. (C) After a 5 h incubation, ThT fluorescence intensities were detected in solutions containing Aβ and exosomes, untreated or pretreated with EGCase. Each column represents the average ± S.D. of four values.

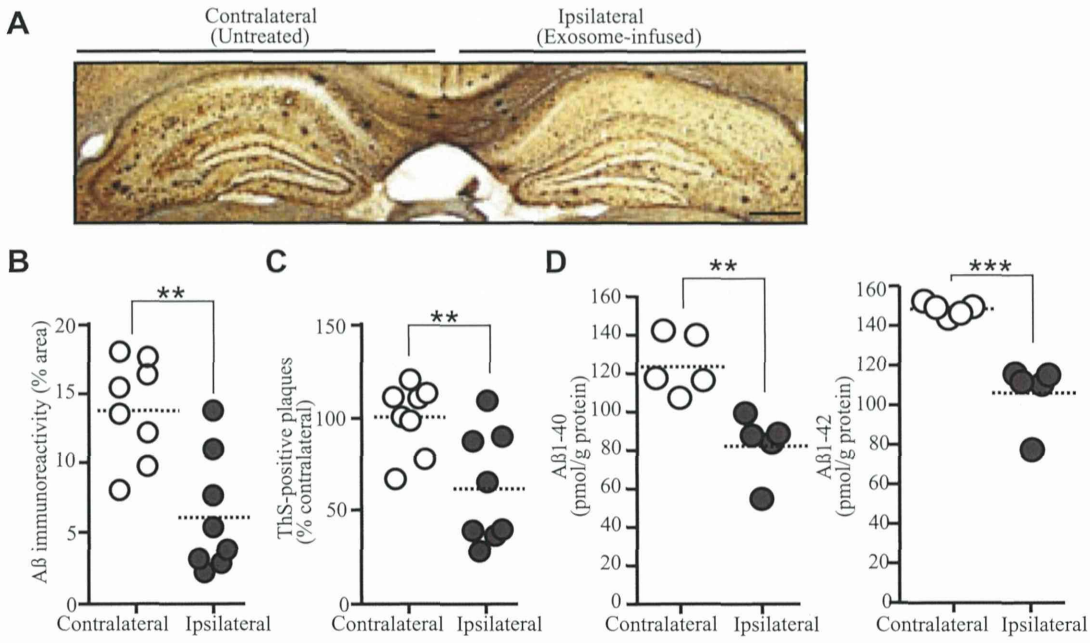


**Fig. 4.** Neuronal exosomes decreases Aβ pathology in APP mouse brains. Neuronal exosomes were infused into the hippocampus of 13-month-old APP mice for 14 days. (A) Image of Aβ-stained hippocampal section. Bar, 200 μm. (B and C) Aβ-immunopositive areas (B) and the numbers of ThS-positive plaques (C) in each hippocampal region were measured ($n = 4$ animals, 2 sections per brain; $^{**}P < 0.01$). (D) Hippocampal Aβs were analyzed by ELISA. ($n = 5$ animals; $^{**}P < 0.01$, $^{***}P < 0.001$).

expression of Rab GTPases, which are responsible for the endosome transport [13,14]. In addition, the dysfunction of dynein, a microtubule-associated protein active in endosome trafficking, has also been observed in aged monkey brains [13]. Notably, knockdown of dynein reduced exosome release from N2a cells [13]. Considering the appearance of endocytic pathology in early AD pathogenesis [15,16], disturbance of intracellular transport might mediate the reduction of exosomes, eventually leading to Aβ accumulation in the aged brains.

Our study reported here clearly demonstrated that intracerebral infusion of neuronal exosomes results in decreases in Aβ levels and amyloid deposition in the brains of APP transgenic mice (Fig. 4). It is noteworthy that another pathological agent of AD, tau, can be collected from the CSF-exosomes of early AD patients [17], raising the possibility that exosomes modulate multiple factors associated with AD pathogenesis. The improvement of endogenous exosome generation might serve as a novel approach for treating or preserving AD.

## Acknowledgements

This work was supported by Creation of Innovation Centers for Advanced Interdisciplinary Research Areas Program, Ministry of Education, Culture, Sports, Science and Technology, Japan.

## Appendix A. Supplementary data

Supplementary data associated with this article can be found, in the online version, at http://dx.doi.org/10.1016/j.febslet.2014.11.027.

## References

[1] Rajendran, L., Honsho, M., Zahn, T.R., Keller, P., Geiger, K.D., Verkade, P. and Simons, K. (2006) Alzheimer's disease beta-amyloid peptides are released in association with exosomes. Proc. Natl. Acad. Sci. U.S.A. 103, 11172–11177.
[2] Vingtdeux, V., Hamdane, M., Loyens, A., Gele, P., Drobeck, H., Begard, S., Galas, M.C., Delacourte, A., Beauvillain, J.C., Buee, L. and Sergeant, N. (2007) Alkalizing drugs induce accumulation of amyloid precursor protein by-products in luminal vesicles of multivesicular bodies. J. Biol. Chem. 282, 18197–18205.
[3] Yuyama, K., Sun, H., Mitsutake, S. and Igarashi, Y. (2012) Sphingolipid-modulated exosome secretion promotes clearance of amyloid-beta by microglia. J. Biol. Chem. 287, 10977–10989.
[4] Yuyama, K., Sun, H., Sakai, S., Mitsutake, S., Okada, M., Tahara, H., Furukawa, J., Fujitani, N., Shinohara, Y. and Igarashi, Y. (2014) Decreased amyloid-beta pathologies by intracerebral loading of glycosphingolipid-enriched exosomes in Alzheimer model mice. J. Biol. Chem. 289, 24488–24498.
[5] Tsuchida, J., Yoshida, T., Sankai, T. and Yasutomi, Y. (2008) Maternal behavior of laboratory-born, individually reared long-tailed macaques (*Macaca fascicularis*). J. Am. Assoc. Lab. Anim. Sci.: JAALAS 47, 29–34.
[6] DeMattos, R.B., Bales, K.R., Parsadanian, M., O'Dell, M.A., Foss, E.M., Paul, S.M. and Holtzman, D.M. (2002) Plaque-associated disruption of CSF and plasma amyloid-beta (Abeta) equilibrium in a mouse model of Alzheimer's disease. J. Neurochem. 81, 229–236.
[7] Gottfried-Blackmore, A., Sierra, A., Jellinck, P.H., McEwen, B.S. and Bulloch, K. (2008) Brain microglia express steroid-converting enzymes in the mouse. J. Steroid Biochem. Mol. Biol. 109, 96–107.
[8] Liu, H.T., Tashmukhamedov, B.A., Inoue, H., Okada, Y. and Sabirov, R.Z. (2006) Roles of two types of anion channels in glutamate release from mouse astrocytes under ischemic or osmotic stress. Glia 54, 343–357.
[9] Heuer, E., Rosen, R.F., Cintron, A. and Walker, L.C. (2012) Nonhuman primate models of Alzheimer-like cerebral proteopathy. Curr. Pharm. Des. 18, 1159–1169.
[10] Oikawa, N., Kimura, N. and Yanagisawa, K. (2010) Alzheimer-type tau pathology in advanced aged nonhuman primate brains harboring substantial amyloid deposition. Brain Res. 1315, 137–149.
[11] Kimura, N., Yanagisawa, K., Terao, K., Ono, F., Sakakibara, I., Ishii, Y., Kyuwa, S. and Yoshikawa, Y. (2005) Age-related changes of intracellular Abeta in cynomolgus monkey brains. Neuropathol. Appl. Neurobiol. 31, 170–180.
[12] Thery, C., 2011. Exosomes: secreted vesicles and intercellular communications. F1000 Biol, Rep., 3, 15.
[13] Kimura, N., Inoue, M., Okabayashi, S., Ono, F. and Negishi, T. (2009) Dynein dysfunction induces endocytic pathology accompanied by an increase in Rab GTPases: a potential mechanism underlying age-dependent endocytic dysfunction. J. Biol. Chem. 284, 31291–31302.
[14] Kimura, N., Okabayashi, S. and Ono, F. (2014) Dynein dysfunction disrupts beta-amyloid clearance in astrocytes through endocytic disturbances. Neuroreport 25, 514–520.
[15] Cataldo, A.M., Barnett, J.L., Pieroni, C. and Nixon, R.A. (1997) Increased neuronal endocytosis and protease delivery to early endosomes in sporadic Alzheimer's disease: neuropathologic evidence for a mechanism of increased beta-amyloidogenesis. J. Neurosci. 17, 6142–6151.
[16] Cataldo, A.M., Petanceska, S., Terio, N.B., Peterhoff, C.M., Durham, R., Mercken, M., Mehta, P.D., Buxbaum, J., Haroutunian, V. and Nixon, R.A. (2004) Abeta localization in abnormal endosomes: association with earliest Abeta elevations in AD and Down syndrome. Neurobiol. Aging 25, 1263–1272.
[17] Saman, S., Kim, W., Raya, M., Visnick, Y., Miro, S., Jackson, B., McKee, A.C., Alvarez, V.E., Lee, N.C. and Hall, G.F. (2012) Exosome-associated tau is secreted in tauopathy models and is selectively phosphorylated in cerebrospinal fluid in early Alzheimer disease. J. Biol. Chem. 287, 3842–3849.

OPEN ACCESS Freely available online

PLOS | ONE

# Infection with *Porphyromonas gingivalis* Exacerbates Endothelial Injury in Obese Mice

**Min Ao[1,2]*, Mutsumi Miyauchi[1]*, Toshihiro Inubushi[1], Masae Kitagawa[3], Hisako Furusho[1], Toshinori Ando[1], Nurina Febriyanti Ayuningtyas[1], Atsuhiro Nagasaki[1], Kazuyuki Ishihara[4], Hidetoshi Tahara[5], Katsuyuki Kozai[2], Takashi Takata[1]***

**1** Department of Oral and Maxillofacial Pathobiology, Institute of Biomedical and Health Sciences, Hiroshima University, Hiroshima, Japan, **2** Department of Pediatric Dentistry, Institute of Biomedical and Health Sciences, Hiroshima University, Hiroshima, Japan, **3** Center of Oral Clinical Examination, Hiroshima University Hospital, Hiroshima University, Hiroshima, Japan, **4** Department of Microbiology, Tokyo Dental College, Tokyo, Japan, **5** Department of Cellular and Molecular Biology, Institute of Biomedical and Health Sciences, Hiroshima University, Hiroshima, Japan

## Abstract

***Background:*** A number of studies have revealed a link between chronic periodontitis and cardiovascular disease in obese patients. However, there is little information about the influence of periodontitis-associated bacteria, *Porphyromonas gingivalis* (*Pg*), on pathogenesis of atherosclerosis in obesity.

***Methods:*** *In vivo* experiment: *C57BL/6J* mice were fed with a high-fat diet (HFD) or normal chow diet (CD), as a control. *Pg* was infected from the pulp chamber. At 6 weeks post-infection, histological and immunohistochemical analysis of aortal tissues was performed. *In vitro* experiment: hTERT-immortalized human umbilical vein endothelial cells (HuhT1) were used to assess the effect of *Pg*/*Pg*-LPS on free fatty acid (FFA) induced endothelial cells apoptosis and regulation of cytokine gene expression.

***Results:*** Weaker staining of CD31 and increased numbers of TUNEL positive cells in aortal tissue of HFD mice indicated endothelial injury. *Pg* infection exacerbated the endothelial injury. Immunohistochemically, *Pg* was detected deep in the smooth muscle of the aorta, and the number of *Pg* cells in the aortal wall was higher in HFD mice than in CD mice. Moreover, *in vitro*, FFA treatment induced apoptosis in HuhT1 cells and exposure to *Pg*-LPS increased this effect. In addition, *Pg* and *Pg*-LPS both attenuated cytokine production in HuhT1 cells stimulated by palmitate.

***Conclusions:*** Dental infection of *Pg* may contribute to pathogenesis of atherosclerosis by accelerating FFA-induced endothelial injury.

**Citation:** Ao M, Miyauchi M, Inubushi T, Kitagawa M, Furusho H, et al. (2014) Infection with *Porphyromonas gingivalis* Exacerbates Endothelial Injury in Obese Mice. PLoS ONE 9(10): e110519. doi:10.1371/journal.pone.0110519

**Editor:** Salomon Amar, Boston University, United States of America

**Received** April 3, 2014; **Accepted** September 16, 2014; **Published** October 21, 2014



**Data Availability:** The authors confirm that all data underlying the findings are fully available without restriction. All relevant data are within the paper and its Supporting Information files.

**Funding:** This work was partially supported by Grants-in-Aid for Scientific Research Scientific Research (C). Research Project Number: 25462855. The funder had no role in study design, data collection and analysis, decision to publish, or preparation of the manuscript.

**Competing Interests:** The authors have declared that no competing interests exist.

* Email: ttakata@hiroshima-u.ac.jp

* These authors contributed equally to this work.

## Introduction

Obesity is an independent risk factor for the development of atherosclerosis. Atherosclerosis, characterized by the accumulation of lipids and fibrous elements in the aortal tissues, is the most important contributor to the progress of cardiovascular disease (CVD) [1]. CVD, formerly the leading cause of death and illness in developed countries, has also become a more serious health problem worldwide [2]. While atherosclerosis was formerly considered a simple and relatively passive lipid storage disease, the past decades have seen an increased interest in the role that chronic inflammation may play in triggering atherosclerosis [3]. According to the "response to injury" hypothesis by Ross (1999), the early stage of atherosclerosis is initiated by a chronic inflammatory response of the arterial wall to endothelial injury, which is called endothelial dysfunction, and is caused by hyperlipidemia, elevated plasma homocysteine concentrations, hypertension, and infectious microorganisms [4]. This dysfunction consequently leads to imbalanced blood vessel regulation and enhanced leukocyte adhesion through up-regulation of adhesion molecules, the synthesis of proinflammatory and prothrombotic factors, and oxidative stress [5].

Recently, epidemiological and interventional studies have revealed a link between atherosclerosis and bacterial infections, including *Chlamydia pneumoniae*, *Helicobacter pylori*, and *Porphyromonas gingivalis* (*Pg*) [6–10]. Periodontitis is a chronic infectious/inflammatory disease caused by periodontal pathogens, and *Pg* is one of the primary species related to both chronic

marginal periodontitis and periapical periodontitis [11–13]. Several clinical trials have revealed an association between periodontitis and levels of systemic inflammatory markers and endothelial injury. However, to our knowledge, there is no report to date clarifying the relationship between *Pg* dental infection and endothelial injury in a diet-induced obese mouse model.

In the present study, we analyzed how dental infection by *Pg* affects endothelial injury, the early stage of atherosclerosis that occurs in obesity. To accomplish this, we employed an *in vivo* model where mice with *Pg*-induced periapical periodontitis were maintained on a normal chow diet (CD) or a high fat diet (HFD). Moreover, hTERT-immortalized human umbilical vein endothelial cells (HuhT1) were used to assess the effect of *Pg* whole cell, *Pg*-LPS and/or free fatty acid (FFA), *in vitro*. We report that HFD results in endothelial injury in mice aortal tissues, and *Pg* infection exacerbates this effect. In parallel, *in vitro* experiments similarly demonstrate that *Pg* whole cell and *Pg*-LPS up-regulates cytokine expression and increases apoptosis of FFA-treated HuhT1 cells. These findings suggest that dental infection by *Pg* promotes endothelial injury in the context of obesity.

## Materials and Methods

### Animal studies

This study was carried out in strict accordance with the recommendations in the Guide for the Care and Use of Laboratory Animals of the Hiroshima University Animal Research Committee and AVMA Guidelines on Euthanasia. The protocol described below was approved by the Committee on the Ethics of Animal Experiments of the Hiroshima University (Permit Number: A09-89). All mice were housed in a specific pathogen free facility in 12 hr light-dark cycles with access to water *ad libitum*.

A total number of 24 5-week-old male SPF *C57BL/6J* mice (Charles River Japan, Inc., Yokohama, Japan) were randomly divided into two groups, fed either a normal chow diet (CD) or a high fat diet (HFD-60; Oriental Yeast Co., Ltd., Tokyo, Japan). After establishment of the obese mouse model by 12 weeks of HFD feeding, mice were further divided into two subgroups (N = 6 each): Mice in the HFD-*Pg* group were infected by *Pg* (as detailed below), while the HFD-NC group served as the negative control without infection. Similarly, the CD group was subdivided and further treated to make CD-NC and CD-*Pg* groups.

### *Pg* infection

All surgeries were performed on mice under intraperitoneal anesthesia induced by pentobarbital sodium (1.62 mg/30 g; Kyoritsu Seiyaku Co., Tokyo, Japan) and atropine sulfate (12.5 ug/30 g; Mitsubishi Tanabe Pharma Co., Osaka, Japan). Surgeries were performed in biosafety cabinets of Hiroshima University Animal Facility, and maximum efforts were made to minimize postoperative pain and suffering. To establish dental infection of *Pg*, the pulp chambers of the maxillary first molars on the left and right sides were opened with a #1/2 round bur. After removing the coronal pulp, a small sterile cotton swab including 1 μl of absorbed bacterial suspension ($10^7$ CFU of *Pg* W83 strain) was inserted into the pulp chamber, which was then sealed with Caviton (GC Co., Tokyo, Japan). Six weeks later, mice were euthanized and samples of maxilla and 5 mm length of aortal tissues from descending aorta at the level equivalent to heart were harvested. Tissues were stored at −80°C for further evaluation or processed as formalin-fixed paraffin embedded (FFPE) samples.

### Immunohistochemistry

Immunolocalization of *Pg* in the aortal wall was examined by using rabbit antiserum against *Pg* whole cell (1:1,000 dilution). Anti-mouse CD-31 monoclonal antibody (1:100 dilution; Dianova GmbH, Hamburg, Germany) was used for immunohistochemical detection of endothelial cells. Immunohistochemical staining was performed using a high polymer method (Histofine Max-PO: Nichirei Biosciences, Tokyo, Japan). Specificity was ascertained by substituting PBS or serum for each primary antibody. Sections were analyzed under light microscopy and photomicrographs obtained at 400x magnification.

### Terminal deoxynucleotidyl transferase dUTP nick end labeling (TUNEL)

To measure *in situ* apoptosis, TUNEL staining was performed on aortal tissues obtained from each group. Tissue samples were processed using an In Situ Apoptosis Detection Kit (Trevigen Inc., Gaithersburg, MD, USA) according to manufacturer's instructions. Negative controls were obtained for each sample by omission of incubation with the TUNEL reaction mixture. Sections were analyzed under light microscopy and photomicrographs were obtained at 400x magnification.

### Histomorphometric analysis

Analysis was performed on 8 sections of aortal tissue per mouse. *Pg* colonies were immonohistochemically stained (as described above) and the number of brown pigments (i.e., *Pg* colonies) was counted under a microscope. The average number of colonies for each group was calculated. The ratio (%) of CD31-positive length per total length of the inner surface of the aortal wall was calculated after immunohistochemical staining (as described above). The total number of TUNEL-positive endothelial cells on was counted and normalized to the number of positive cells per 1 mm inner surface of aortal wall.

### Identification of *Pg* in aortal tissue by PCR analysis

Total DNA was extracted from mouse aortal tissue by DNeasy Tissue Kit (QIAGEN Science, Germantown, MD, USA) according to the manufacturer's instructions. The *mgl* gene that encodes l-methionine-α-deamino-γ-mercaptomethane-lyase (METase) and specifically identifies *Pg* [14] was amplified by PCR. The primer pair used was 5′-GCTATCGAGAACGCCTTC-3′ (Forward) and 5′-GCAGTGCCATCTGCTTCT-3′ (reverse). Genomic DNA of the *Pg* W83 strain was used as a positive control template.

### Cell culture and treatment

hTERT-immortalized human umbilical vein endothelial cells (HuhT1) were used in this study. HuhT1 cells were previously established by transfection with human telomerase reverse transcriptase [15]. HuhT1 cells were maintained in HuMedia-EG2 growth medium with a commercial supplemental kit (Kurabo, Osaka, Japan). $1.5\times10^5$ of HuhT1 cells were inoculated to a 35 mm collagen coated dish for the following experiments. 10 mM palmitate (Sigma, Hamburg, Germany) per 1% Bovine Serum Albumin (BSA) stock solution was prepared according to the method of Wobser [16]. FFA-free-BSA-treated cells were used as negative control. Before each treatment, medium was completely removed, cells were washed with PBS, and culture medium was replaced a fresh batch. Lipopolysaccharide of *Pg* (*Pg*-LPS, Strain ATCC 33277) was purchased from InvivoGen and a concentration of 100 ng/ml was used. Cells were maintained at 37°C in a normal atmosphere containing 5% $CO_2$.

### Flow cytometry

Huht1 cells were plated on 60 mm dishes at a density of $4\times10^6$. Cells were treated with 100 uM palmitate or 1 ug/ml Doxorubicin (Dox, positive control of apoptosis) for 12 h. PE Annexin V apoptosis Detection Kit1 (BD Pharmingen) was used according to the instruction of manufacture. In brief, cells were washed twice with ice-cold PBS, resuspended in 50 ul binding buffer, added Annexin V-PE (2.5 ul) and 7AAD (2.5 ul) and mixed gently. Incubation was performed at room temperature avoiding light for 15 min. Binding buffer (400 ul) was added to each sample and proceeded to flow cytometry analysis.

### Antibiotic protection assay

HuhT1 cells were pre-incubated with palmitate (50 μM) for 12 h. Before *Pg* infection, culture media were replaced by an antibiotic-free medium for at least 2 h, followed by gentle rinsing three times with PBS. Cells were exposed to *Pg* at a multiplicity of infection (MOI) of 100 for 2 h, and then incubated with metronidazole (200 μg/ml) and gentamicin (300 μg/ml) for 1 h to kill extracellular bacteria [17]. Cells were permeated with 1 ml of sterile, nonpyrogenic distilled water for 20 min and 100 μl of 10x diluent was plated on blood agar supplemented with 10% defibrinated sheep blood, hemin (5 μg/ml), and menadione (0.5 μg/ml), and cultured under anaerobic conditions (Anaeropack system, Mitsubishi Gas Chemical Co., Tokyo, Japan) at 37°C. The number of intracellular invaded *Pg* cells was determined by colony counting on blood agar plates.

### Cell counting

After 12 h pre-incubating with or without palmitate (50 μM), HuhT1 cells were treated with *Pg*-LPS (100 ng/ml) for an additional 12 h. The number of floating versus attached cells was determined by a cell counting machine (Z1, Coulter, Hialeah, FL, USA) in order to calculate the percentage of dead (floating) cells in the total number.

### RT-PCR

HuhT1 cells ($1.5\times10^5$ cells) were pre-incubated with palmitate (50 μM) for 12 h. After 1 h of treatment with *Pg*-LPS (100 ng/ml), total RNA was extracted from the cell pellets using the RNeasy Mini Kit (Qiagen, K.K., Tokyo, Japan) following the manufacturer's instructions. RNA concentration and purity were determined by spectrophotometry. 1 μg of total RNA was used for cDNA synthesis using the ReverTra Dash kit (TOYOBO Co., Ltd., Osaka, Japan). Aliquots of total cDNA were amplified with Go Taq Green Master Mix (Promega), and amplifications for COX-2 and TNF-α were performed in a MyCycler thermal cycler (BIO-RAD, Tokyo, Japan) for 30 cycles (30 s denaturation at 94°C, 30 s annealing at 58°C, and 1 min extension at 72°C) for all primers. GAPDH was used as an internal control. The amplification reaction products were resolved on 1.5% agarose/TAE gels (Nacalaitesque, Inc., Kyoto, Japan), electrophoresed at 100 mV, and visualized by ethidium-bromide staining. PCR primer pairs were COX-2: 5′-TGAGCATCTACGGTTTGCTG-3′ (Forward) and 5′-TGCTTGTCTGGAACAACTGC-3′ (Reverse); TNF-α: 5′-TCCTTCAGACACCCTCAACC-3′ (Forward) and 5′-AGGCCCCAGTTTGAATTCTT-3′ (Reverse); GAPDH: 5′-TGAACGGGAAGCTCACTGG-3′ (Forward) and 5′-TCCACCACCCTGTTGCTGTA-3′ (Reverse).

### Western blotting

After 12 h of pre-incubation with or without palmitate (50 μM), cells were treated with *Pg*-LPS (100 ng/ml) for another 12 h. Cells were also pretreated by TLR4 signaling inhibitor Cli-095 (InvivoGen, San Diego, CA, USA) for 6 h and stimulated by palmiatate (50 μM) for indicated time. Primary antibodies against Polyclonal anti-poly (ADP-ribose) polymerase (PARP), P-p65, P-p38, P-JNK and P-ERK were purchased from Cell Signaling Technology, Inc. (Danvers, MA, USA). Monoclonal anti-β-actin was purchased from Sigma-Aldrich Co. LLC. (St. Louis, MO, USA) Western blotting was performed as previously described [18]. Cell pellets ($1.5\times10^5$ cells) were resuspended in ice-cold lysis buffer. Proteins were separated by SDS-PAGE and electro-blotted onto a nitrocellulose membrane. After blocking of the membrane with 3% milk for 30 min, membranes were incubated with primary antibodies (1:1000) and anti-rabbit secondary antibody. β-actin (1:10,000) was used as internal control. The results were visualized by Amersham ECL western blotting detection system (GE Healthcare, Japan).

### Immunofluorescent staining

HuhT1 cells grown on coverslips were fixed in 4% paraformaldehyde for 10 min at room temperature, rinsed three times with ice-cold PBS and then permeabilized in 0.1% Triton X-100 in PBS for 10 min at room temperature. After rinsing three times with PBS, the coverslips were incubated with primary antibody against *Pg* in 10% DMEM for 2 h at room temperature, rinsed three times with PBS and then incubated with anti-rabbit Alexa488 (1:1000, Molecular Probes, Eugene, OR, USA), which functioned as the secondary antibody. DNA was visualized by DAPI staining (blue) and F-actin was visualized by Phalloidin staining (red). Pictures were recorded using Keyence BZ-8100 series All-in-one Fluorescence Microscope (KEYENCE Japan, Osaka, Japan).

### Statistical analysis

Results are reported as mean ± standard deviation (SD). Intergroup statistical differences were evaluated by student t-test or Mann-Whitney test, with the level of significance set at $P<0.01$ and $P<0.05$.

## Results

### Dental *Pg* infection induces periapical granuloma (Figure 1)

In both groups of *Pg* infected mice, CD-*Pg* and HFD-*Pg*, severe pulp necrosis was observed in the first upper molars six weeks after infection. Periapical granulomas were apparent, and pulp chambers were infiltrated with neutrophils and macrophages (Figure 1A). *Pg* colonies were located in infected pulp chambers (Figure 1B), and bacteria were also present in associated neutrophils and macrophages (Figure 1C).

### *Pg* exacerbates HFD-induced endothelial injury and apoptosis (Figure 2)

The inner surface of aortal wall is lined by endothelial cells, and no obvious histological changes in aortal walls were apparent among the experimental groups (Figure 2Aa–d). Immunolocalization of endothelial marker CD-31 was used to further assess the condition of endothelium. In the CD-NC group, aortal walls were lined with endothelial cells exhibiting a strong positive reaction for CD-31 (Figure 2Ba), while CD-31 staining of CD-*Pg* aorta was relatively weaker (Figure 2Bb). Furthermore, CD-31 staining was further reduced and more heterogeneous in the HFD-NC group, indicating damage to the endothelial layer (Figure 2Bc). *Pg* infection further exacerbated this effect, as CD-31 expression

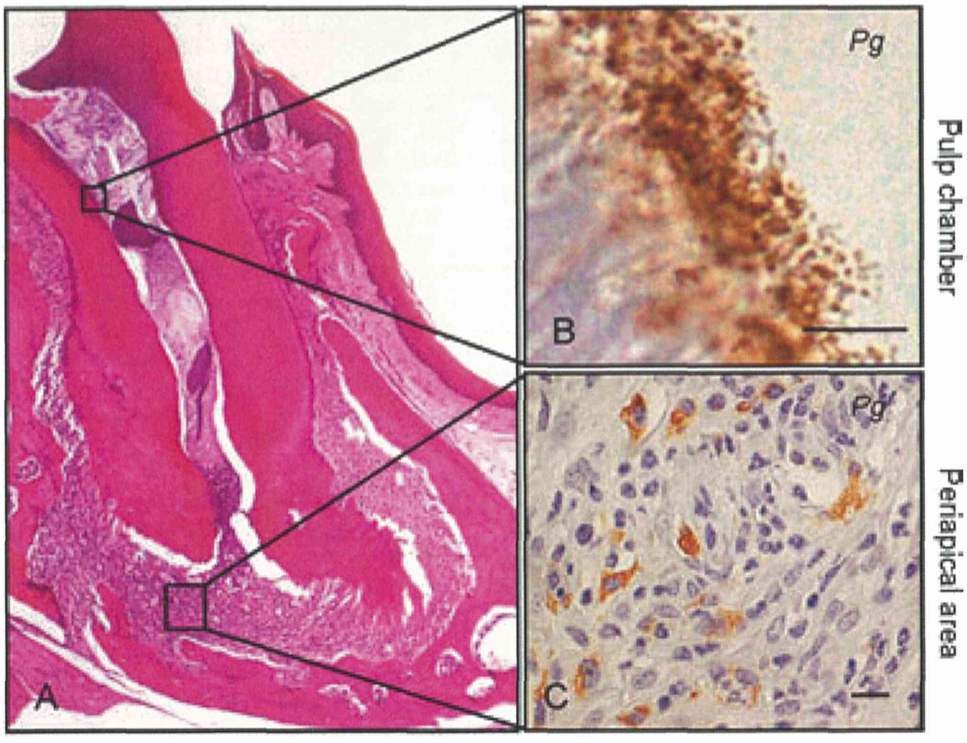


**Figure 1. Dental *Pg* infection induces periapical granuloma.** Severe pulp necrosis is observed in the first upper molars after six weeks of *Pg* infection. (A) Periapical granuloma is a representative histological feature of *Pg* infected molars, and is infiltrated with neutrophils and macrophages. (B) Immunohistochemical staining shows *Pg* colonies (brown pigment) in the pulp chambers and (C) in neutrophils and macrophages in the periapical area. Scale bar, 10 μm. *Pg, Porphyromonas gingivalis.* Experiments were performed three times or more with similar results.
doi:10.1371/journal.pone.0110519.g001

was observed to be much weaker and discontinuous in HFD-*Pg* (Figure 2B-d). These observations were supported by quantitative analysis of the ratio of CD31-positive endothelial surface over the total length measured (Figure 2C). CD31-positive surfaces were significantly reduced in HFD groups compared to CD groups and *Pg* infection significantly reduced CD-31 positive surfaces in both the CD ($P<0.01$) and HFD ($P<0.05$) groups.

TUNEL staining was used to detect apoptosis in cells of the aortal tissues. No positive reactions were observed in cells in the CD-NC and CD-*Pg* groups (Figure 2Da, b). In HFD groups, TUNEL-positive nuclei were seen in endothelial cells and smooth muscle cells of the aortal wall. The positive reaction in HFD-*Pg* was stronger than that in HFD-NC (Figure 2Dc, d), and the number of TUNEL positive cells was significantly higher in HFD-*Pg* versus HFD-NC ($P<0.05$) (Figure 2E).

## Dental *Pg* infection predisposes to increased invasion of injured mouse aortal tissue under HFD conditions (Figure 3)

In these studies, we induced periapical periodontitis by application of live *Pg* cultures into root canals of mouse first molars. Interestingly, *Pg* DNA and *Pg* colonies were detected in aortal tissues at 6 weeks post treatment (Figure 3A and B). In Figure 3A, the *Pg*-specific *mgl* gene was detected by PCR in DNA harvested from the aortal wall of both CD-*Pg* and HFD-*Pg* groups, but not in NC groups. In the *Pg*-infected CD group, *Pg* colonies were immunohistochemically detected in the surface layer of the intima (Figure 3Bb), whereas in the HFD group, *Pg* could be observed in the deeper smooth muscle layer of the aorta (Figure 3Bd). Moreover, the number of *Pg* colonies detected in aorta sections was significantly higher ($P<0.01$) in the HFD group versus the CD group (Figure 3C).

## *Pg* and *Pg*-LPS increase palmitate-induced apoptosis in HuhT1 cells (Figure 4)

We used hTERT-immortalized human umbilical vein endothelial cells (HuhT1) as a model to explore the effects of *Pg*-LPS *in vitro*. Previously, we demonstrated up-regulation of serum LPS in both CD-*Pg* and HFD-*Pg* groups [20]. Therefore, we examined the combined effects on HuhT1cells of *Pg*-LPS and palmitate, a representative FFA that is elevated as a result of obesity-induced endothelial injury. In cells untreated by palmitate, there were no significant morphological changes in HuhT1 cells, except for slight cell shrinkage after *Pg*-LPS or *Pg* whole cell treatment (Figure 4A a, b, c). In contrast, palmitate treatment caused marked cell shrinkage and triggered cells to detach from dishes (Figure 4Ad). Palmitate pre-treatment followed by addition of *Pg*-LPS or *Pg* whole cell induced more severe cell detachment, however, the effect of Pg whole cell was not as robust as Pg-LPS (Figure 4A e, f). Quantification of these observations confirmed that in the NC group, palmitate treatment induced a 1.7-fold increase in floating cells compared to the untreated group ($P<0.01$). *Pg*-LPS stimulation alone did not induce significant cell detachment, whereas, *Pg*-LPS in combination with palmitate induced a significant 2.5-fold increase in floating cells over palmitate-untreated cells ($P<0.01$). Similarly, *Pg* whole cell treatment induced 2.0-fold increase in floating cells with palmitate+ vs palmitate- treatment (Figure 4B). Flow cytometry detected 24.37% of cells treated by palmitate undergoing early apoptosis with higher affinity to Annexin V compared to 8.72% in

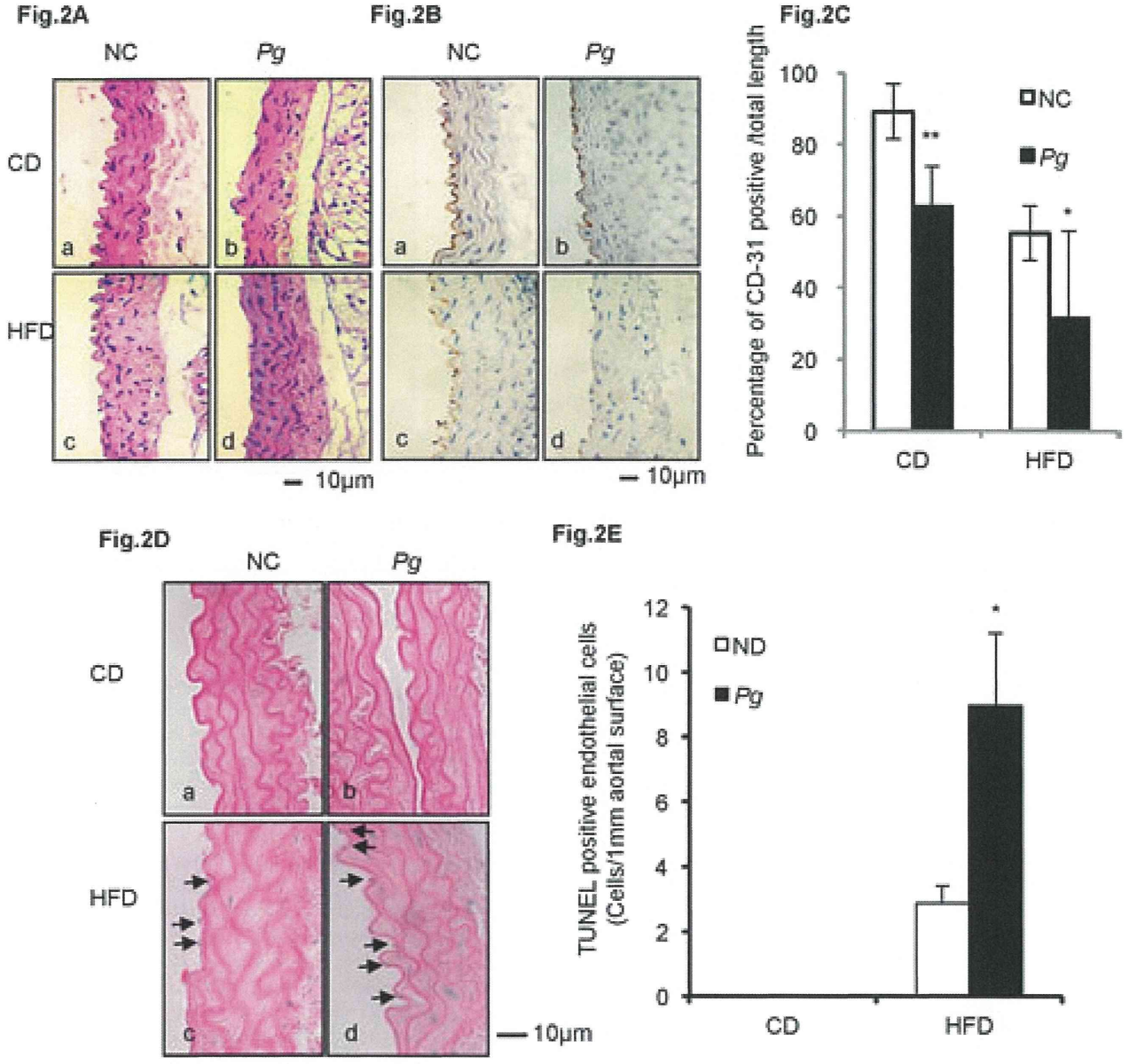


**Figure 2. *Pg* exacerbates HFD-induced endothelial injury and apoptosis.** (A) Histological findings in aortal tissue in CD mice (a, b) and in HFD mice (c, d). H&E, scale bar, 100 μm. (B) IHC staining of CD-31 (endothelial cell marker) in aortal tissue in CD mice (a, b) and in HFD mice (c, d). Scale bar, 10 μm. (C) Percentage of aortal surface covered by CD31-positive endothelial cells in the HFD-*Pg* group is significantly lower than that of the HFD-NC group. Mean ± SD *P<0.05, **P<0.01. (D) TUNEL staining of aortal tissue in CD mice (a, b) and in HFD mice (c, d). Scale bar, 10 μm. (E) Number of TUNEL-positive cells per unit length of aortal surface in HFD-*Pg* group is significantly higher than that of HFD-NC group. Mean ± SD *P< 0.05. CD, chow diet; HFD, high fat diet; NC, negative control; *Pg, Porphyromonas gingivalis.* Experiments were performed three times or more with similar results.
doi:10.1371/journal.pone.0110519.g002

non-treated cells (Figure 4C). Dox served as positive control (Figure 4A, 4B, 4C).

Poly (ADP-ribose) polymerase (PARP) cleavage is an established and reliable apoptosis indicator downstream of caspase family activation, especially caspase 3 and caspase 7. To determine potential induction of apoptosis of HuhT1 cells by palmitate treatment, we examined PARP cleavage at the protein level. After 12 h of palmitate stimulation, a dose-dependent PARP cleavage was observed, detectable at the low dose of 50 μM (Figure 4D). A time course revealed that PARP was cleaved by 12 h after 50 μM palmitate treatment (Figure 4E), a time point at which substantial numbers of cells were observed to be detached (data not shown) and likely undergoing apoptosis. Furthermore, *Pg*-LPS treatment increased palmitate-induced PARP cleavage (Figure 4F).

## *Pg* and *Pg*-LPS up-regulate COX-2 and TNF-α expression in palmitate treated HuhT1 cells via activated TLR4 (Figure 5)

We next investigated effects of palmitate priming on cells. Palmitate induced phosphorylation of p65 and p38 as early as 15 min and ERK at 45 min after treatment. 6 h pretreatment Toll-like receptor-4 (TLR4) inhibitor, Cli-095, prevented phosphorylation of p65 and p38 at early time point induced by